

MAY 29 1997

SANDIA REPORT

SAND97-1176 • UC-406

Unlimited Release

Printed May 1997

RECEIVED

JUN 01 1997

OSTI

Advanced Tomographic Flow Diagnostics for Opaque Multiphase Fluids

J. R. Torczynski, T. J. O'Hern, D. R. Adkins, N. B. Jackson, K. A. Shollenberger

Prepared by
Sandia National Laboratories
Albuquerque, New Mexico 87185 and Livermore, California 94550

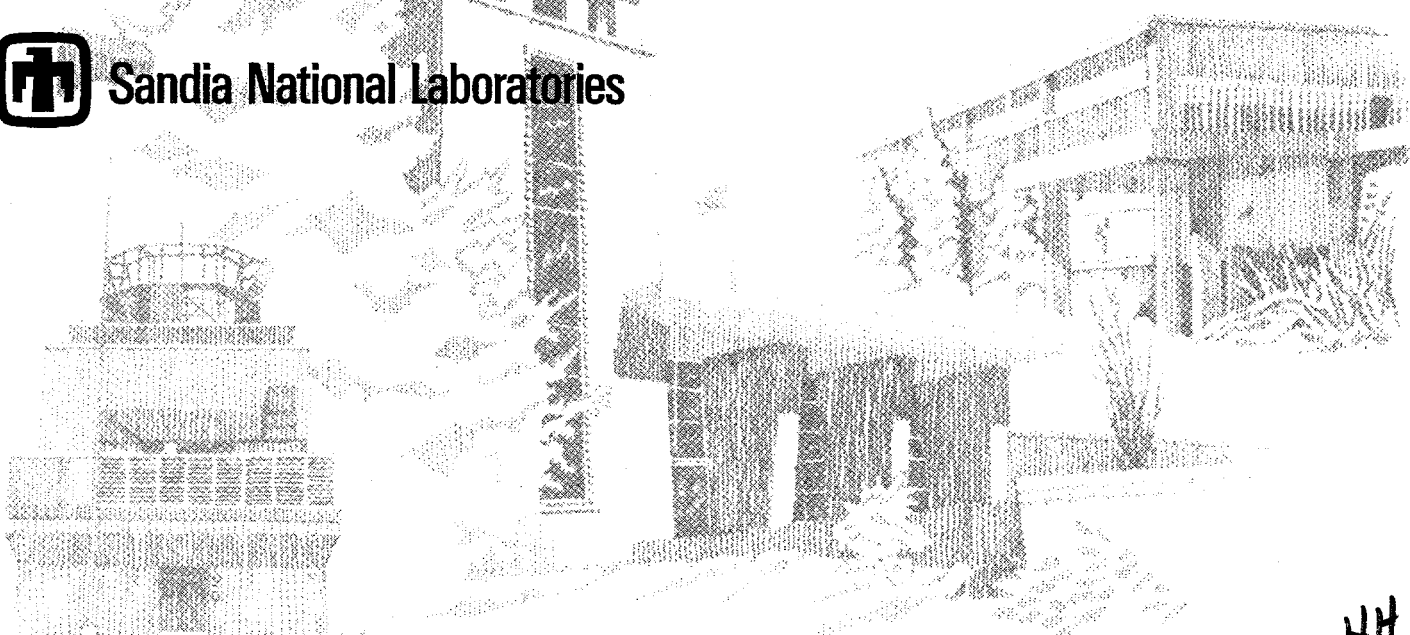
Sandia is a multiprogram laboratory operated by Sandia Corporation,
a Lockheed Martin Company, for the United States Department of
Energy under Contract DE-AC04-94AL85000.

MASTER

Approved for public release; distribution is unlimited.



Sandia National Laboratories



HH

Issued by Sandia National Laboratories, operated for the United States Department of Energy by Sandia Corporation.

NOTICE: This report was prepared as an account of work sponsored by an agency of the United States Government. Neither the United States Government nor any agency thereof, nor any of their employees, nor any of their contractors, subcontractors, or their employees, makes any warranty, express or implied, or assumes any legal liability or responsibility for the accuracy, completeness, or usefulness of any information, apparatus, product, or process disclosed, or represents that its use would not infringe privately owned rights. Reference herein to any specific commercial product, process, or service by trade name, trademark, manufacturer, or otherwise, does not necessarily constitute or imply its endorsement, recommendation, or favoring by the United States Government, any agency thereof, or any of their contractors or subcontractors. The views and opinions expressed herein do not necessarily state or reflect those of the United States Government, any agency thereof, or any of their contractors.

Printed in the United States of America. This report has been reproduced directly from the best available copy.

Available to DOE and DOE contractors from
Office of Scientific and Technical Information
P.O. Box 62
Oak Ridge, TN 37831

Prices available from (615) 576-8401, FTS 626-8401

Available to the public from
National Technical Information Service
U.S. Department of Commerce
5285 Port Royal Rd
Springfield, VA 22161

NTIS price codes
Printed copy: A03
Microfiche copy: A01

DISCLAIMER

This report was prepared as an account of work sponsored by an agency of the United States Government. Neither the United States Government nor any agency thereof, nor any of their employees, make any warranty, express or implied, or assumes any legal liability or responsibility for the accuracy, completeness, or usefulness of any information, apparatus, product, or process disclosed, or represents that its use would not infringe privately owned rights. Reference herein to any specific commercial product, process, or service by trade name, trademark, manufacturer, or otherwise does not necessarily constitute or imply its endorsement, recommendation, or favoring by the United States Government or any agency thereof. The views and opinions of authors expressed herein do not necessarily state or reflect those of the United States Government or any agency thereof.

DISCLAIMER

**Portions of this document may be illegible
in electronic image products. Images are
produced from the best available original
document.**

Advanced Tomographic Flow Diagnostics for Opaque Multiphase Fluids

J. R. Torczynski¹, T. J. O'Hern¹, D. R. Adkins¹, N. B. Jackson², K. A. Shollenberger¹

¹Engineering Sciences Center

²Advanced Energy Technology Center

Sandia National Laboratories

P. O. Box 5800

Albuquerque, New Mexico 87185-0834

Abstract

This report documents the work performed for the "Advanced Tomographic Flow Diagnostics for Opaque Multiphase Fluids" LDRD (Laboratory-Directed Research and Development) project and is presented as the fulfillment of the LDRD reporting requirement. Dispersed multiphase flows, particularly gas-liquid flows, are industrially important to the chemical and applied-energy industries, where bubble-column reactors are employed for chemical synthesis and waste treatment. Due to the large range of length scales (10^{-6} - 10^1 m) inherent in real systems, direct numerical simulation is not possible at present, so computational simulations are forced to use models of subgrid-scale processes, the accuracy of which strongly impacts simulation fidelity. The development and validation of such subgrid-scale models requires data sets at representative conditions. The ideal measurement techniques would provide spatially and temporally resolved full-field measurements of the distributions of all phases, their velocity fields, and additional associated quantities such as pressure and temperature. No technique or set of techniques is known that satisfies this requirement. In this study, efforts are focused on characterizing the spatial distribution of the phases in two-phase gas-liquid flow and in three-phase gas-liquid-solid flow. Due to its industrial importance, the bubble-column geometry is selected for diagnostics development and assessment. Two bubble-column testbeds are utilized: one at laboratory scale and one close to industrial scale. Several techniques for measuring the phase distributions at conditions of industrial interest are examined: level-rise measurements, differential-pressure measurements, bulk electrical impedance measurements, electrical bubble probes, x-ray tomography, gamma-densitometry tomography, and electrical impedance tomography. The first four techniques provide either spatially averaged or local information and are discussed in the context of validation. Although already well developed, the fifth technique is not suitable for large-scale flow experiments but is useful for validation efforts. The last two techniques are investigated and discussed in detail, and representative phase-distribution results are presented for gas-liquid and gas-liquid-solid flows in the two testbeds at conditions of interest.

Acknowledgment

The authors gratefully acknowledge interactions with the following individuals. Dr. Bernard A. Toseland and Dr. Bharat L. Bhatt of Air Products and Chemicals, Inc. provided much valuable information about the characteristics of industrial-scale bubble columns. Prof. Steven L. Ceccio, Dr. Ann L. Tassin-Leger, and Mr. Darin L. George of the University of Michigan collaborated closely on the development and application of electrical techniques for measuring phase volume fractions. Prof. Milorad P. Dudukovic of Washington University provided valuable insight into multiphase-flow diagnostics and the development of appropriate test beds for validation. Dr. Georges L. Chahine and Dr. Ramani Duraiswami of Dynaflo, Inc. developed the boundary-element method electrical-impedance tomography code which was compared to the finite-element method code discussed herein. Dr. Bryan A. (Bucky) Kashiwa and Dr. W. Brian VanderHeyden of Los Alamos National Laboratory graciously provided information about their CFDLIB numerical simulations of bubble-column flow. Dr. William R. Howell of the Dow Chemical Company continually encouraged the authors to broaden their outlook and consider other classes of multiphase flows. Gerald C. Stoker and Kyle R. Thompson of Sandia National Laboratories performed the x-ray tomography analyses of various experiments. The authors particularly acknowledge the excellent technical support of Mr. Thomas W. Grasser, Mr. John J. O'Hare, and Mr. C. Buddy Lafferty of Sandia National Laboratories, without whose capable assistance the experiments could not have been performed. Dr. Arthur C. Ratzel of Sandia National Laboratories is thanked for his exemplary management of this effort.

Table of Contents

Table of Contents	5
List of Figures	7
List of Tables	9
Nomenclature	11
1. Introduction	14
1.1. Overview	14
1.2. Motivation	14
1.3. Slurry Bubble-Column Reactors (SBCRs)	18
1.4. Scope of Existing and Proposed Diagnostics	21
2. Diagnostic Techniques	23
2.1. Techniques Yielding Spatially-Averaged or Local Information	23
2.1.1. Level-Rise (LR) Technique	23
2.1.2. Differential-Pressure (DP) Technique	24
2.1.3. Bulk Electrical Impedance (BEI) Technique	26
2.1.4. Electrical Bubble Probe (EBP)	27
2.2. X-Ray Tomography (XRT) and Real-Time Radiography (RTR) Techniques	30
2.2.1. XRT System	30
2.2.2. RTR System	31
2.3. Gamma-Densitometry Tomography (GDT) Technique	31
2.3.1. GDT System	32
2.3.2. GDT Reconstruction Algorithm	39
2.4. Electrical-Impedance Tomography (EIT) Technique	41
2.4.1. EIT System	42
2.4.2. EIT Reconstruction Algorithm: Overview	45
2.4.3. EIT Reconstruction Algorithm: Theory	48
2.4.4. EIT Reconstruction Algorithm: FEMEIT Implementation	52
2.4.5. EIT Reconstruction Algorithm: FEMEIT Validation	55
2.4.6. EIT Reconstruction Algorithm: Extensions	59
3. Preliminary Validation Efforts	61
3.1. Wax/Catalyst (WCD) Experiments	61
3.1.1. WCD Description	61
3.1.2. WCD Experimental Results from XRT	62
3.2. Boxed Bubble Column (BBC) Experiment	65
3.2.1. BBC Experimental Setup	66
3.2.2. BBC Experimental Results from RTR	67
3.3. Insulating Cylindrical Inclusion (ICI) Experiments	69
3.3.1. ICI Experimental Setup	69
3.3.2. ICI Experimental Results from EIT	70
4. Experimental Testbeds and Results	72
4.1. Transparent Bubble Column (TBC) Experiment	72
4.1.1. TBC Experimental Setup	73

4.1.2.	TBC Experimental Results.....	75
4.2.	Slurry Bubble-Column Reactor (SBCR) Experiment.....	79
4.2.1.	SBCR Experimental Setup.....	80
4.2.2.	SBCR Experimental Results.....	80
4.3.	Two-Phase Experiments Combining GDT and EIT.....	84
4.3.1.	Liquid-Solid Flow (LSF) Experiment.....	85
4.4.	Application of GDT and EIT to TBC.....	89
5.	Conclusions.....	93
A.	FEMEIT Files.....	94
	References.....	96
	Distribution.....	102

List of Figures

Figure 1.	Nondilute turbulent gas-liquid flow.....	15
Figure 2.	Terminal velocity of an isolated air bubble in water (Jamialahmadi et al., 1994).	16
Figure 3.	Los Alamos CFDLIB calculation of bubble-column flow (Kumar et al., 1995b).	17
Figure 4.	Slurry bubble-column reactor (SBCR) schematic diagram.	19
Figure 5.	SBCR photograph and process diagram, courtesy of Air Products and Chemicals.	20
Figure 6.	Schematic diagram of level-rise (LR) technique.	24
Figure 7.	Schematic diagram of differential-pressure (DP) technique.	25
Figure 8.	Bulk electrical impedance (BEI) probe ring with two rectangular electrodes.	26
Figure 9.	Electrical bubble probe (EBP) schematic, bubble interceptions, and rms correlation. .	28
Figure 10.	Gas volume fraction radial distributions from EBP.	29
Figure 11.	X-ray tomography (XRT) experimental setup.	30
Figure 12.	Gamma-densitometry tomography (GDT) system.	32
Figure 13.	A detector erroneously observes some of the scattered gamma photons.	33
Figure 14.	Schematic diagram of traverse for source and detector.	34
Figure 15.	Gamma spectrum from the MCA with various features identified.	35
Figure 16.	Gamma spectra from the MCA with various thicknesses of water.	37
Figure 17.	Logarithmic gamma spectra (points) and peak-fitting algorithm (curves).	38
Figure 18.	Schematic diagram of Abel transform geometry.	39
Figure 19.	Schematic diagram of electrical-impedance tomography (EIT).	41
Figure 20.	Block diagram of EIT hardware.	42
Figure 21.	EIT strip and point electrodes and probe-ring installations.	44
Figure 22.	Schematic diagram of EIT.	45
Figure 23.	Linearity allows all EIT solutions to be built up from fewer solutions.	47
Figure 24.	EIT mesh refinement studies. Good convergence is observed.	56
Figure 25.	2DynaEIT (Duraiswami et al., 1995) and FEMEIT ICI reconstructions.	58
Figure 26.	EIT determination of radius of an ICI using point electrodes and EITA3D.	60
Figure 27.	Wax/catalyst disk (WCD) samples with hole patterns.	61
Figure 28.	XRT resolution study for "large-signature" WCD.	63
Figure 29.	XRT resolution study for "quadrant calibration" WCD.	64
Figure 30.	Boxed bubble-column experiment.	66
Figure 31.	Schematic diagram of RTR applied to BBC experiment.	67
Figure 32.	RTR results for BBC experiment.	68
Figure 33.	Schematic diagram of EIT with an insulating cylindrical inclusion (ICI).	69
Figure 34.	EIT reconstructions of insulating cylinders using strip electrodes.	71
Figure 35.	The transparent bubble-column (TBC) experiment.	72
Figure 36.	Sparger (final design) in TBC.	73
Figure 37.	Temperature-dependent electrical conductivity can give spurious results.	74
Figure 38.	Count-rate results from GDT in TBC.	75
Figure 39.	Gas-liquid and gas-liquid-solid results from GDT in TBC.	77
Figure 40.	Phase volume fraction results from GDT in TBC.	78
Figure 41.	The slurry bubble-column reactor (SBCR) experiment.	79

Figure 42. Gas volume fraction results from DP for gas-liquid flow in SBCR..... 81
Figure 43. Gas volume fraction results from GDT for gas-liquid flow in SBCR..... 82
Figure 44. Gas volume fraction vertical variation from DP and GDT in SBCR..... 84
Figure 45. The liquid-solid flow (LSF) experiment..... 86
Figure 46. Solid volume fraction results from GDT and EIT in LSF. 88
Figure 47. GDT and EIT installed in TBC for measuring gas-liquid flow. 90
Figure 48. GDT and EIT results at same conditions in TBC..... 91

List of Tables

Table 1.	Nondimensionalization employed in EIT theoretical development.....	47
Table 2.	EITA3D reconstructions of ICI diameters.	70
Table 3.	Average gas volume fractions in TBC.	76
Table 4.	Average gas volume fraction values from GDT and DP for air-water in SBCR.	83
Table 5.	Conditions and results for LSF experiment.....	87

